Journal for ImmunoTherapy of Cancer

Inhibiting CMTM4 reverses the immunosuppressive function of myeloid-derived suppressor cells and augments immunotherapy response in cervical cancer

Jianyi Ding,[1] Haoran Hu,[1] Yashi Zhu,[1] Xinxin Xu,[1] Bo Yin,[1] Meiqin Yang,[1] Huijuan Zhou,[1] Tiefeng Huang,[2] Mengjie Li,[2] Yifan Kou,[2] Zilale Rahim,[2] Baoyou Huang,[1,3] Ang Li,[1,4] Wei Wang,[1] Lingfei Han [1,2]

To cite: Ding J, Hu H, Zhu Y, *et al*. Inhibiting CMTM4 reverses the immunosuppressive function of myeloid-derived suppressor cells and augments immunotherapy response in cervical cancer. *Journal for ImmunoTherapy of Cancer* 2025;**13**:e011776. doi:10.1136/jitc-2025-011776

► Additional supplemental material is published online only. To view, please visit the journal online (https://doi.org/10.1136/jitc-2025-011776).

JD, HH and YZ contributed equally.

JD, HH and YZ are joint first authors.

Accepted 22 May 2025

For numbered affiliations see end of article.

Correspondence to
Professor Ang Li;
liang@tongji.edu.cn

Professor Wei Wang;
2405132@tongji.edu.cn

Professor Lingfei Han;
lingfeihan@tongji.edu.cn

ABSTRACT

CKLF (chemokine-like factor)-like MARVEL transmembrane domain-containing family member 4 (CMTM4), belonging to the CMTM family of transmembrane domain proteins, plays a significant role in the initiation, progression, and metastasis of cancer. Nevertheless, its involvement in tumor immunity remains elusive. In the present investigation, we observed an upregulation of CMTM4 expression in patients with cervical cancer (CC), which also serves as a prognostic indicator for patients with CC. In vitro experiments and therapeutic models have demonstrated that CMTM4 upregulates the expansion of myeloid-derived suppressor cells (MDSCs) in the tumor microenvironment via the CCL2 (C–C motif chemokine ligand 2)/CCR2 (C–C motif chemokine ligand 2) and IL-6 (interleukin-6)/GP130 (glycoprotein 130) axes. This process exerts immunosuppressive effects and promotes the occurrence and progression of CC. Mechanistically, CMTM4 interacts and stabilizes PHB2 (prohibitin 2) through post-translational modification, which further induces activation of the STING (stimulator of interferon genes)/TBK1 (TANK-binding kinase 1)/STAT6 (signal transducer and activator of transcription 6) pathway, facilitating the nuclear translocation of STAT6 which binds to the CCL2/IL-6 promoter, leading to the upregulation of CCL2/IL-6 transcription expression. Importantly, targeting CMTM4 with CMTM4-small interfering RNA enhanced the effectiveness of anti-programmed cell death protein 1 (anti-PD-1) therapy. Our study identifies CMTM4 as a crucial determinant guiding the homing of MDSCs to CC, thereby contributing to MDSCs-mediated immune suppression and tumor progression. The combination of CMTM4 inhibition and anti-PD-1 treatment shows promising antitumor efficacy against CC. These findings offer novel insights into the tumor microenvironment and have the potential to inform the development of innovative immunotherapy approaches for CC.

WHAT IS ALREADY KNOWN ON THIS TOPIC

⇒ Immune checkpoint blockade (ICB) plays a critical role in the treatment of recurrent cervical cancer, but its clinical efficacy remains limited. CKLF (chemokine-like factor)-like MARVEL transmembrane domain-containing family member 4 (CMTM4) has been recognized for its role in regulating programmed death-ligand 1 (PD-L1) stability within the tumor immune microenvironment. However, the immunological functions of CMTM4 beyond PD-L1 regulation, particularly in cervical cancer, remain to be fully characterized.

WHAT THIS STUDY ADDS

⇒ This study demonstrates that CMTM4 promotes immunosuppression by recruiting myeloid-derived suppressor cells (MDSCs) via the CCL2/CCR2 axis and promoting their differentiation through IL-6/GP130 signaling. Notably, CMTM4 inhibition enhances the therapeutic efficacy of anti-programmed cell death protein 1 (anti-PD-1) treatment by restoring antitumor immune responses.

HOW THIS STUDY MIGHT AFFECT RESEARCH, PRACTICE OR POLICY

⇒ These findings identify CMTM4 as a critical immunosuppressive regulator in cervical cancer. Targeting CMTM4 may represent a promising combinatorial strategy with ICB to overcome resistance to immunotherapy and improve clinical outcomes in patients with recurrent cervical cancer.

⇒ Significance: CMTM4 regulates cervical cancer progression by modulating MDSCs through the CCL2/CCR2 and IL-6/GP130 axes, and serves as a potential therapeutic target to enhance anti-PD-1 immunotherapy efficacy.

INTRODUCTION

Cervical cancer (CC) stands as one of the most prevalent malignancies affecting the female reproductive system. Worldwide, it holds the fourth position in terms of both incidence and mortality among females.[1] Immunotherapy, notably immune checkpoint blockade (ICB)

therapy, has emerged as a highly promising approach for tumor treatment. Currently, the efficacy of ICB therapy is constrained in CC, and immunotherapy has not attained the status of a standard treatment option. A significant contributing factor is the immune incompetence frequently observed in the immune system of patients with CC. This state hampers the activation of effective cellular and humoral responses required for the clearance of cancerous cells and the virus.[2] Consequently, enhancing fundamental research on the immune escape mechanisms of CC holds paramount importance in enhancing the efficacy of immunotherapy for CC.

The CKLF-like MARVEL transmembrane domain-containing family (CMTM) represents a recently recognized international gene family, comprised of nine genes, including chemokine-like factor (CKLF) and CKLFSF1–8 (CKLF superfamily members 1–8) in humans.[3] CMTM4, belonging to the CKLFSF, exhibits highly conserved gene sequences with three types of RNA splicing bodies. The v1 and v2 isoforms are ubiquitously expressed in the membranes and cytoplasm of various tissues and cells.[4] A 2017 study demonstrated the critical role of CMTM4 and CMTM6 as proteins regulating the stability of programmed death-ligand 1 (PD-L1). They enhance the expression of both inducible and constitutive PD-L1 on the cell membrane by safeguarding PD-L1 from degradation mediated by 26S protease or lysosomes.[5 6] Consequently, CMTM4 and CMTM6 employ programmed cell death protein 1 (PD-1)/PD-L1 signaling to suppress effector T cells within the tumor microenvironment (TME), evading attacks from the immune system.[7–10] CMTM4 and CMTM6 exhibit a 55% sequence similarity. Notably, CMTM6 exhibits correlations with immune-associated pathways, infiltration of immune cells, and the expression of a majority of genes related to the immune response within TME. This suggests a potential crucial role for CMTM6 in modulating TME.[8 11 12] However, the specific contribution of CMTM4 to TME remains to be fully elucidated.

The accumulation of immunosuppressive cell populations within the TME imparts immunosuppressive characteristics, contributing to the suboptimal efficacy of immunotherapy in patients with cancer. Myeloid-derived suppressor cells (MDSCs) constitute a heterogeneous population of myeloid progenitor cells that accumulate in the TME, serving as potent mediators in suppressing T-cell function and promoting immune evasion.[13] Activated MDSCs serve as a source of secreted cytokines and enzymes that inhibit T cells and natural killer (NK) cells while activating regulatory T cells (Tregs).[14] Nonetheless, the signals and mechanisms governing MDSCs activity and recruitment in CC remain unclear.

In this study, in both mouse tumor models of CC and patient cases, we discovered significant overexpression of CMTM4, which promotes CC occurrence and development. This protein targets PHB2 (prohibitin 2) and activates the STING (stimulator of interferon genes)/TBK1 (TANK-binding kinase 1)/STAT6 (signal transducer and activator of transcription 6) pathway, facilitating STAT6 binding to the CCL2/IL-6 promoter. Consequently, this process promotes the recruitment and activation of MDSCs through the CCL2 (C–C motif chemokine ligand 2)/CCR2 (C–C motif chemokine ligand 2) and IL-6 (interleukin-6)/GP130 (glycoprotein 130) axis within TME, exerting immunosuppressive effects. Finally, we found that targeting CMTM4 in CC could enhance the efficacy of ICB therapy for patients. These findings unveil the mechanism of immune escape mediated by CMTM4 and present potential therapeutic targets for immunotherapy in CC.

RESULTS

CMTM4 mediates the evolution of CC through immune-related mechanisms

There is currently no relevant research investigating the role of the CMTM family in CC. Notably, CMTM4/6 showed higher expression than other members in CC (figure 1A). CMTM4 (but not CMTM6) was specifically upregulated in cervical cancer cells (figure 1B), and high CMTM4 (but not CMTM6) correlated with worse patient survival significantly (figure 1C,D). These findings suggest a pivotal role of CMTM4 in CC progression.

Further analysis revealed that CMTM4 overexpression in CC cell lines compared with ECT (figure 1E) and in tumor tissues compared with controls (figure 1F). Subsequent clinical correlation analysis showed that CMTM4 expression was significantly associated with tumor size in patients with CC (online supplemental table 1). Immunohistochemical (IHC) analysis revealed higher CMTM4 in CIN (cervical intraepithelial neoplasia) than normal epithelium but lower than in cervical squamous cell carcinoma (CSC), cervical adenocarcinoma, and cervical adenocarcinoma squamous cell carcinoma (figure 1G). When compared with paracancerous tissues, cancer tissues exhibited significant overexpression of CMTM4, as evidenced by both IHC (figure 1G) and western blot (WB) (figure 1H). As the clinical staging advances for CIN and CSC (figure 1I), there is a corresponding increase in the expression of CMTM4.

To further investigate the role of CMTM4 in CC, we used CRISPR-Cas9 (Clustered Regularly Interspaced Short Palindromic Repeats–CRISPR-associated protein 9) to knockout CMTM4 (C4KO) in HeLa, SiHa, and TC1 (figure 1J, online supplemental figure 1A). CMTM4 knockout inhibited cell proliferation and migration in vitro (online supplemental figure 1B–D), and severely attenuated TC1 allograft growth in immunocompetent mice (C57/BL6) (figure 1K). Interestingly, the antitumor effect of C4KO was diminished in immunodeficient mice (NCG), suggesting CMTM4 promotes CC primarily via immune regulation (figure 1L). These findings demonstrate CMTM4's oncogenic role through antitumor immunity modulation.

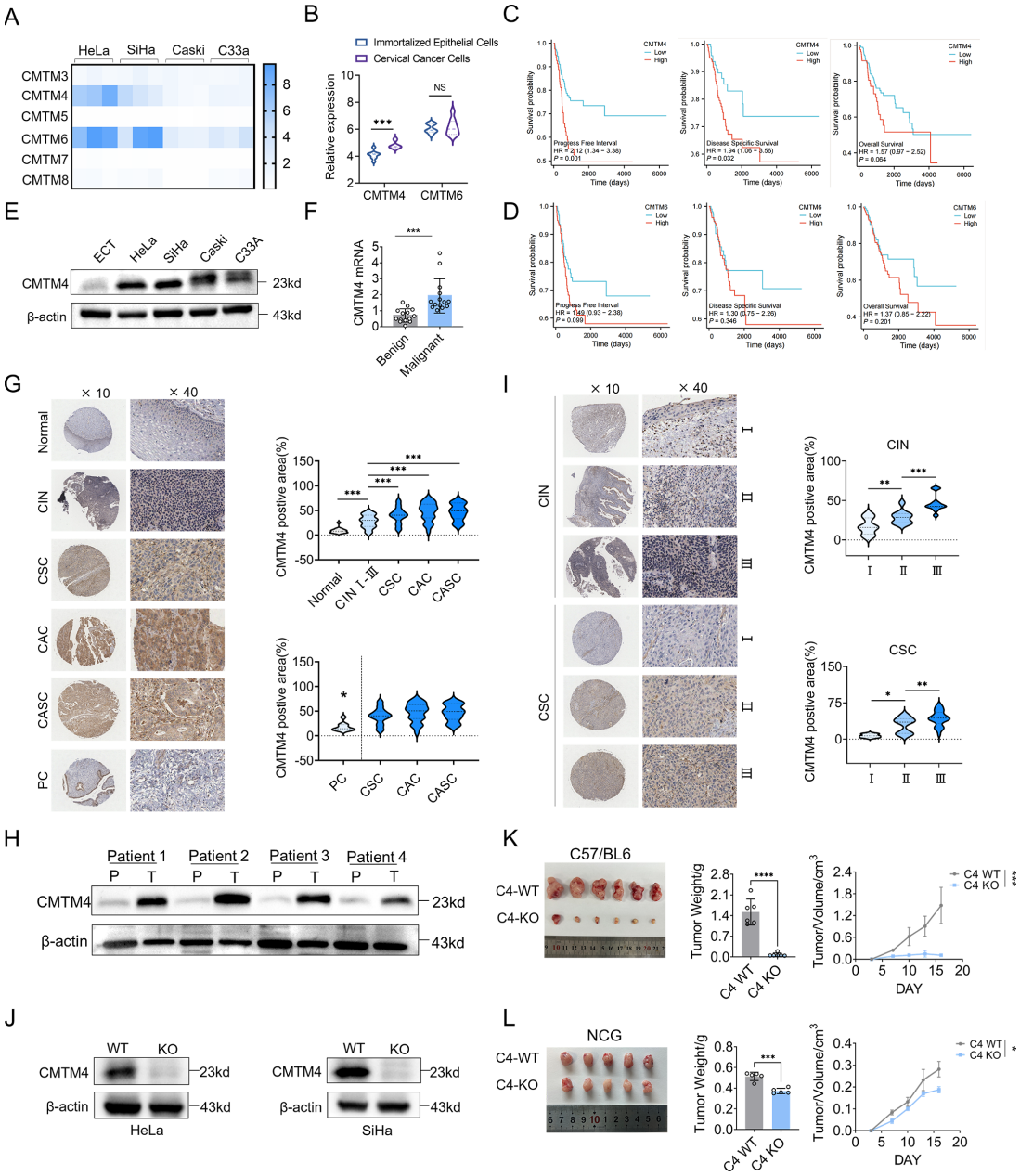

Figure 1 CMTM4 is highly expressed in CC and mediates its malignant biological behaviors. (A) Heatmap of CMTM3–8 of mRNA expression in cervical cancer cells. (B) Cancer Cell Line Encyclopedia database analysis of CMTM4 and CMTM6 expression in normal cervical epithelium and cervical cancer cell lines. (C–D) TCGA survival analysis of high CMTM4 (C) or CMTM6 (D) expression. (E) WB analysis of CMTM4 expression in normal cervical epithelial cells and cervical cancer cells. (F) CMTM4 expression in benign controls (n=14) and cervical cancer (n=14). (G) Immunohistochemical staining of human cervical tissue arrays using specific antibodies for CMTM4. Scale bar for×10 images: 200 µm; scale bar for×40 images: 50 µm. Statistical diagram (above) of positive proportion of CMTM4 in normal cervical epithelial cells (n=16), CSC (n=32), CAC (n=41) and CASC (n=40). Statistical diagram (below) of the positive proportion of CMTM4 in paracancerous tissues and tumor tissues. (H) WB analysis of CMTM4 expression in cervical cancer tissues and adjacent normal tissues. p, paracancerous tissues; T, tumor tissues. (I), immunohistochemical staining of I–III stages of CIN (left) or CSC (right) using specific antibodies for CMTM4. Scale bar for×10 images: 200 µm; scale bar for×40 images: 50 µm. Statistical diagram of the positive proportion of CMTM4 in I (n=13), II (n=10), III (n=11) stages of CIN. Statistical diagram of the positive proportion of CMTM4 in I (n=3), II (n=18), III (n=25) stages of CSC. (J) Knockout of CMTM4 in HeLa, SiHa was examined by WB analysis. (K) Intradermal tumor volume (n=6) of C57/BL6 mice injected with TC1 CMTM4 KO or control cells. Images of TC1 allografts, tumor weight and tumor growth are shown. (L) Intradermal tumor volume (n=5) of NCG mice injected with TC1 CMTM4 KO or control cells. Images of TC1 allografts, tumor weight, and tumor growth are shown. *p<0.05, **p<0.01, ***p<0.001, ****p<0.0001. CAC, cervical adenocarcinoma; CASC, cervical adenocarcinoma squamous cell carcinoma; CC, cervical cancer; CIN,cervical intraepithelial neoplasia; CKLF, chemokine-like factor; CMTM, CKLF-like MARVEL transmembrane domain-containing family; CSC, cervical squamous cell carcinoma; KO, knockout; mRNA, messenger RNA; PC, paracancerous; TCGA, The Cancer Genome Atlas; WB, western blot; WT, wild type.

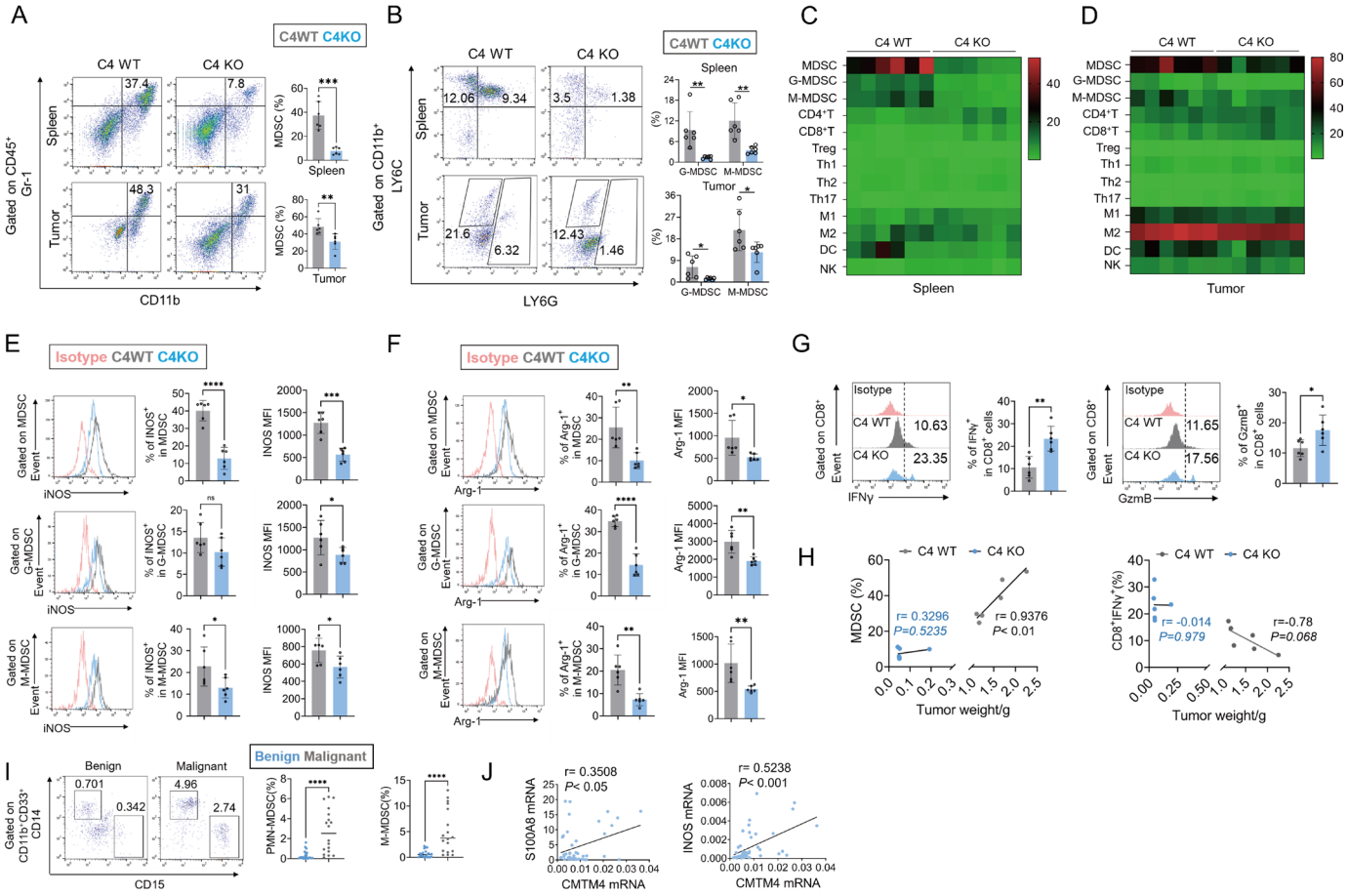

Figure 2 CMTM4 increases MDSCs infiltration and inhibits CD8$^+$ T cell accumulation in CC. (A–B) Flow cytometric anaysis of MDSCs (A), G-MDSC or M-MDSC (B) in TC1-C4KO and TC1-C4WT tumor-bearing mice. (C–D) Composition of immune cells in the TC1 spleen (C) and tumor (D) was shown in the heatmap. (E–F) Flow cytometric analysis of the ability of MDSC, G-MDSC, and M-MDSC to secrete INOS (E) or Arg-1 (F). INOS and Arg-1 expressions were described by percentage and mean fluorescence intensity (MFI). (G) Flow cytometric analysis of the infiltration of IFN-γ and GzmB CD8$^+$ T cells. (H) Correlation between tumor weight with tumorous MDSCs abundance, tumor-infiltrating CD8$^+$ T cells IFN-γ level in TC1-C4KO and TC1-C4WT tumor-bearing mice model (All n=6). (I) Flow cytometric analysis of PMN-MDSC and M-MDSC in PBMCs isolated from patients with benign tumors (n=21) and cervical cancer (n=18). (J) Correlation analysis of S100A8 or INOS expression and CMTM4 expression in clinical samples. *p<0.05, **p<0.01, ***p<0.001, ****p<0.0001. Arg-1, arginase-1; CC, cervical cancer; CKLF, chemokine-like factor; CMTM, CKLF-like MARVEL transmembrane domain-containing family; DC, dendritic cell; G-MDSC, granulocyte-like MDSC; GzmB, granzyme B; IFN, interferon; iNOS, inducible nitric oxide synthase; KO, knockout; MDSC, myeloid-derived suppressor cell; M-MDSC, monocyte-like MDSC; mRNA, messenger RNA; NK, natural killer; PMN-MDSC, polymorphonuclear myeloid-derived suppressor cell; Th1, T helper type 1 cell; Treg, regulatory T cell; WT, wild type.

CMTM4 promotes MDSCs infiltration and inhibits the accumulation of CD8$^+$ T cells in CC

To investigate the potential role of CMTM4 in regulating antitumor immunity in CC, we analyzed immune cell profiles in immunocompetent tumor-bearing mice (figure 2A–D, online supplemental figure 2). Our observations in TC1-C4KO allograft mice revealed enhanced antitumor immunity, characterized by a significant reduction in MDSCs (CD11b$^+$Gr-1$^+$), granulocyte-like MDSCs (G-MDSCs) (CD11b$^+$LY6G^{High}LY6C^{Low}), and monocyte-like MDSCs (M-MDSCs) (CD11b$^+$LY6G^{Low}LY6C^{High}) (figure 2A,B). Additionally, there was a decrease in Tregs (CD4$^+$CD25$^+$FOXP3$^+$) (figure 2C,D, online supplemental figure 2B,J), along with a reduced ability of MDSCs, G-MDSCs, and M-MDSCs to secrete immunosuppressive enzyme INOS (inducible nitric oxide synthase) and Arg-1 (arginase-1) (figure 2E,F). Furthermore, an increase in interferon (IFN)-γ and granzyme B-positive CD8$^+$ T cells was observed in TC1-C4KO allografts, indicating heightened activation of cytotoxic T cells (figure 2G). Notably, in TC1-C4WT allografts, the infiltration of MDSCs showed a significant positive correlation with increasing tumor burden, whereas no such correlation was observed in TC1-C4KO allografts (figure 2H). Similarly, in TC1-C4WT allografts, T-cell infiltration exhibited a more pronounced negative correlation with increasing tumor burden compared with TC1-C4KO allografts, although neither showed statistical significance (figure 2H).

Furthermore, the flow cytometry analysis of patient with CC blood samples demonstrated significantly elevated

proportions of PMN-MDSCs (polymorphonuclear myeloid-derived suppressor cells) ($CD11b^+CD33^+CD15^+$), M-MDSCs (monocytic myeloid-derived suppressor cell) ($CD11b^+CD33^+CD14^+$) and Treg cells compared with benign controls accompanied by reduced $CD8^+IFN\text{-}\gamma^+$ T cell populations (figure 2I, online supplemental figure 3A,B). Additionally, the expression of PMN-MDSC and M-MDSC showed a significant inverse correlation with $CD8^+IFN\text{-}\gamma^+$ T cells and a non-significant positive association with Tregs (online supplemental figure 3C,D). More importantly, real-time quantitative PCR (RT-qPCR) analysis revealed a positive correlation between CMTM4 expression and MDSCs-related immunosuppressive markers in clinical samples (figure 2J).

Our collective findings suggest that CMTM4 primarily regulates MDSCs infiltration, exerting immunosuppressive effects that contribute to the promotion of CC growth.

Knockdown of CMTM4 results in the dysregulation of immune-associated cytokines and chemokines

To investigate how CMTM4 promotes immune suppression through the regulation of MDSCs in CC, gene set enrichment analysis linked CMTM4 to cytokine pathways (online supplemental figure 4A). Additionally, conditioned medium (CM) was collected from HeLa-C4WT and HeLa-C4KO cells to further examine the role of CMTM4 in modulating MDSCs in CC through in vitro functional experiments (online supplemental figure 4B). We found C4KO-CM significantly restrained MDSCs recruitment in Transwell assays (figure 3A,B, (online supplemental figure 3C) and reduced MDSCs differentiation in co-cultures (figure 3C,D). In addition, the C4KO-CM not only inhibited MDSCs differentiation but also led to a downregulation of its ability to secrete immunosuppressive enzymes (figure 3E).

To identify CMTM4-regulated cytokines involved in MDSCs recruitment and activation, we performed Luminex-MultiDTX-43-Human to detect inflammatory and chemokine factors in HeLa-C4WT and HeLa-C4KO CM (figure 3F, online supplemental table 7). Our analysis revealed a significant decrease in the expression of CCL2, IL-6, and VEGF (vascular endothelial growth factor) in HeLa-C4KO cells, which was further validated by RT-qPCR and ELISA in both HeLa and SiHa cells (figure 3G,H, online supplemental figure 4D). Additionally, we observed an upregulation of CXCL10 (C-X-C motif chemokine ligand 10) and CCL5 (C-C motif chemokine ligand 5) expression, which can recruit $CD8^+$ T cells to exert antitumor activity (figure 3F, online supplemental table 7).

Further phenotype analysis in clinical samples revealed significantly elevated serum CCL2/IL-6 levels in patients with CC versus benign controls (figure 3I,J), which positively correlated with PMN-MDSC/M-MDSC proportions (figure 3K,L). Kaplan-Meier analysis revealed that high expression of CCL2/IL-6 was significantly associated with poorer overall survival (figure 3M). Consistent with clinical data, CMTM4 knockout reduced CCL2/IL-6 expression in serum or tumor tissue from TC1 allograft models (figure 3N). Subsequent analysis demonstrated a significant positive correlation between mRNA expression of CMTM4 and IL-6 or CCL2 in clinical specimens (figure 3O). These findings establish CCL2/IL-6 as key mediators of CMTM4-driven MDSCs recruitment in cervical cancer, guiding our subsequent focus on these cytokines.

Pharmacological blockade of the CCL2/CCR2 and IL-6/GP130 axes can inhibit the pro-tumor effects of CMTM4

To further unveil the mechanism of CMTM4 in recruiting MDSCs, we either overexpressed CMTM4 (online supplemental figure 5A) or knocked down CCL2 (online supplemental figure 5B) in HeLa cells. CMTM4 overexpression increased CCL2 secretion and MDSCs migration. However, this effect was abolished by CCL2 knockdown (figure 4A, online supplemental figure 5C–E). Since CCL2 recruits MDSCs via CCR2 binding,[15 16] we examined CCR2 expression and found it significantly elevated on MDSCs from patients with CC (figure 4D). Furthermore, CMTM4 knockout reduced CCR2 expression on splenic MDSCs in mice (figure 4E).

Continuing, to validate the CMTM4-CCL2-CCR2 axis in MDSC chemotaxis, we performed migration assays showing that CMTM4 knockout impaired MDSC migration toward HeLa/TC1-CM, which was restored by recombinant CCL2. CCR2 blockade (RS504393) abolished migration differences between control and C4KO groups (figure 4B,C, online supplemental figure 5F). In the TC1 tumor-bearing model, CCR2 inhibition suppressed control tumor growth but showed no effect on C4KO tumors (figure 4F), accompanied by reduced G-MDSCs and increased Tregs/$CD8^+IFN\text{-}\gamma^+$ T cells in control groups only (figure 4G, online supplemental figure 5G–L). These findings strongly suggest that CMTM4 recruits MDSCs via the CCL2-CCR2 axis and is integral to tumor progression mediated by CMTM4.

Moving forward, we delved into the mechanism by which CMTM4 activates MDSCs through IL-6. IL-6 promotes MDSCs differentiation through its receptor GP130,[17 18] and we found a dose-dependent upregulation of GP130 expression on the surface of monocytes on treatment with IL-6 recombinant factor (figure 4H). In vitro, HeLa-C4KO-CM attenuated MDSCs differentiation, which was rescued by recombinant IL-6 but abolished by GP130 blockade (LMT-28 , a small-molecule inhibitor of the IL-6/GP130 pathway) (figure 4I). Similarly, IL-6 restored while LMT-28 eliminated differences in MDSCs immunosuppressive enzyme secretion between groups (online supplemental figure 6A,B).

In vivo, GP130 inhibition attenuated control tumor growth and modulated immune populations (reduced G-MDSCs and Tregs, increased $CD8^+IFN\text{-}\gamma^+$ T cells), with no effect on C4KO tumors (figure 4J,K, online supplemental figure 6C–H).

These results suggest that CMTM4 promotes MDSCs differentiation through the IL-6-GP130 axis. However,

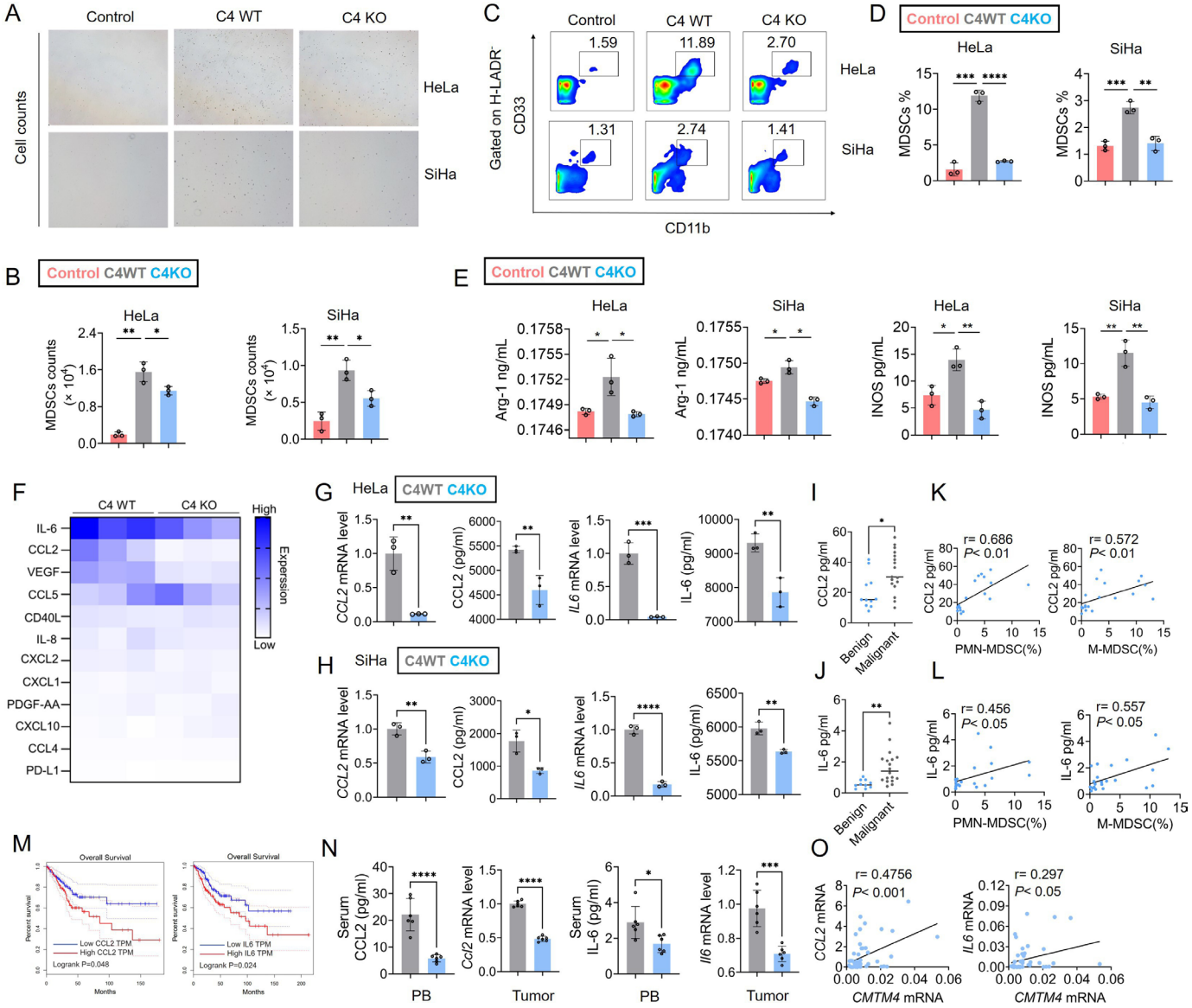

Figure 3 Knockdown of CMTM4 results in the dysregulation of immune-associated cytokines and chemokines. (A–B) CM collected from CMTM4 KO-HeLa and CMTM4 KO-SiHa or from control were placed in the lower chambers. Freshly isolated PBMCs MDSCs were seeded in the upper chambers and allowed to transwell for 24 hours. Total numbers of transwelled MDSCs found in the lower chambers were counted. Data are presented as the mean±SEM (n=3). (C–D) CM collected from CMTM4 KO-HeLa and CMTM4 KO-SiHa or control was cocultured with mononuclear cells from cord blood for 24 hours. The proportion of MDSCs was detected by flow cytometry (n=3). (E) After treating umbilical cord blood mononuclear cells with CM from CMTM4 KO HeLa and CMTM4 KO SiHa or the control group for 24 hours, the coculture supernatant was collected and the secretion of Arg-1 or INOS was detected by ELISA. (F) Heatmap of 43 different human cytokine expression levels with a concentration greater than 100 pg/mL in CMTM4 KO-HeLa and CMTM4 NC-HeLa using Luminex-MultiDTX-43-Human. (G–H) RT-qPCR and ELISA assays analyze expression of IL-6 and CCL2 in CMTM4 KO-HeLa and CMTM4 KO-SiHa (n=3). (I–J) ELISA analysis of CCL2 and IL-6 expression in the serum of patients with benign tumors (CCL2 n=17; IL-6 n=10) and cervical cancer (CCL2 n=11; IL-6 n=18). (K–L) Correlation analysis of PMN-MDSC or M-MDSC expression and CCL2 or IL-6 expression in clinical samples. (M) GEPIA overall survival curves analysis of patients with CC with high or low expression of CCL2 or IL-6. N. Tumor mRNA level and serum protein concentration of CCL2 and IL-6 in TC1 tumor-bearing mice models (n=6). (O) Correlation analysis of CCL2 or IL-6 mRNA expression and CMTM4 mRNA expression in clinical cervical tissue. *p<0.05, **p<0.01, ***p<0.001, ****p<0.0001. Arg-1, arginase-1; CCL, C-C motif chemokine ligand; CM, conditioned medium; CKLF, chemokine-like factor; CMTM, CKLF-like MARVEL transmembrane domain-containing family; CXCL, C-X-C motif chemokine ligand; GEPIA, Gene Expression Profiling Interactive Analysis; IL-6, interleukin-6; iNOS, inducible nitric oxide synthase; KO, knockout; MDSC, myeloid-derived suppressor cell; mRNA, messenger RNA; PB, peripheral blood; PBMCs, peripheral blood mononuclear cells; PDGF-AA, platelet-derived growth factor-AA; PD-L1, programmed death-ligand 1; RT-qPCR, real-time quantitative PCR; Th1, T helper type 1 cell; TPM, transcripts per million; WT, wild type.

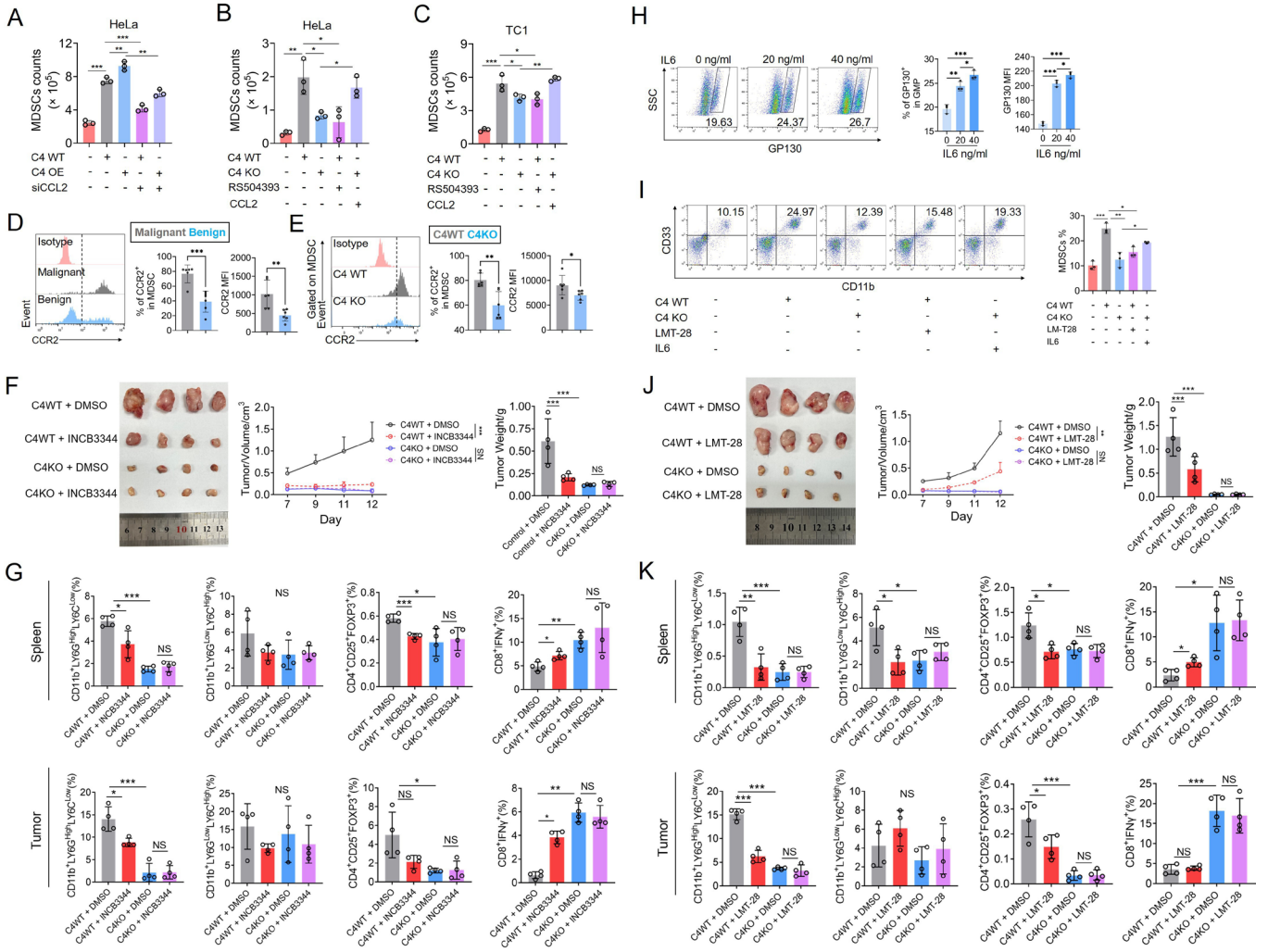

Figure 4 CMTM4 facilitates CCL2/CCR2-mediated MDSCs chemotaxis and IL-6/GP130-induced MDSCs differentiation. (A) MDSCs were seeded in the top chamber of the transwell containing 100 µL RPMI medium and the CM derived from different groups placed in the bottom. (B–C) MDSCs were seeded in the top chamber of the transwell containing 100 µL RPMI medium with or without CCR2 inhibitor (RS504393, 10 mM) in CMTM4-NC HeLa or CMTM4-NC TC1 group. On the other hand, the bottom chamber contained 600 µL of CMTM4-KO HeLa or CMTM4-KO TC1 CM with or without recombinant CCL2 protein (1 ng/mL). After 24-hour incubation, cells that have completely migrated to the bottom chamber were counted (n=3). (D) Flow cytometric analysis of CCR2 expression on PBMCs derived MDSCs in patients with benign tumors (n=6) and cervical cancer (n=6). CCR2 expressions were described by percentage and MFI. (E) Flow cytometric analysis of CCR2 expression on tumor-bearing mice-derived MDSCs in spleen. CCR2 expressions were described by percentage and MFI (n=6). (F) Tumor growth in mice intradermally injected with TC1 CMTM4 KO cells or control cells and treated with INCB3344 (10 mg/kg body weight) or DMSO daily following tumor inoculation. Images of TC1 allografts, tumor growth tumor, and weight are shown (n=4). (G) Flow cytometric analysis of G-MDSC, M-MDSC, Treg, and $CD8^+IFN\text{-}\gamma^+$ T cells in the treated tumor-bearing mice models. Data are presented as the mean±SEM (n=4). (H) Flow cytometric analysis of GP130 expression on cord blood mononuclear cells treated with IL-6 recombinant factor at different concentrations. GP130 expression was described by percentage and MFI (n=3). I. CM collected from CMTM4 NC-HeLa with or without GP130 inhibitor (LMT-28, 10 mM) and CMTM4 KO-HeLa with or without recombinant IL-6 protein (40 ng/mL) were cocultured with mononuclear cells from cord blood for 24 hours. Each group is treated by GM-CSF (40 ng/mL). The proportion of MDSCs was detected by flow cytometry. Data are presented as the mean±SEM (n=3). (J) Tumor growth in mice intradermally injected with TC1 CMTM4 KO cells or control cells and treated with LMT-28 (10 mg/kg body weight) or DMSO daily following tumor inoculation. Images of TC1 allografts, tumor growth tumor, and weight are shown (n=4). (K) Flow cytometric analysis of G-MDSC, M-MDSC, Treg, and $CD8^+IFN\text{-}\gamma^+$ T cells in the treated tumor-bearing mice models. Data are presented as the mean±SEM (n=4). *p<0.05, **p<0.01, ***p<0.001. NS, not significant. CCL2, C-C motif chemokine ligand 2; CCR2, C-C motif chemokine receptor 2; CM, conditioned medium; CKLF, chemokine-like factor; CMTM, CKLF-like MARVEL transmembrane domain-containing family; DMSO, dimethyl sulfoxide; G-MDSC, granulocyte-like MDSC; GM-CSF, granulocyte-macrophage colony-stimulating factor; GMP, granulocyte–monocyte progenitor; GP130, glycoprotein 130; IFN, interferon; IL-6, interleukin-6; KO, knockout; LMT-28, small-molecule inhibitor of the IL-6/GP130 signaling pathway; MDSC, myeloid-derived suppressor cell; MFI, mean fluorescence intensity; M-MDSC, monocyte-like MDSC; OE, overexpression; PBMCs, peripheral blood mononuclear cells; RPMI, Roswell Park Memorial Institute medium; siCCL2, small interfering RNA targeting CCL2; Treg, regulatory T cell; WT, wild type.

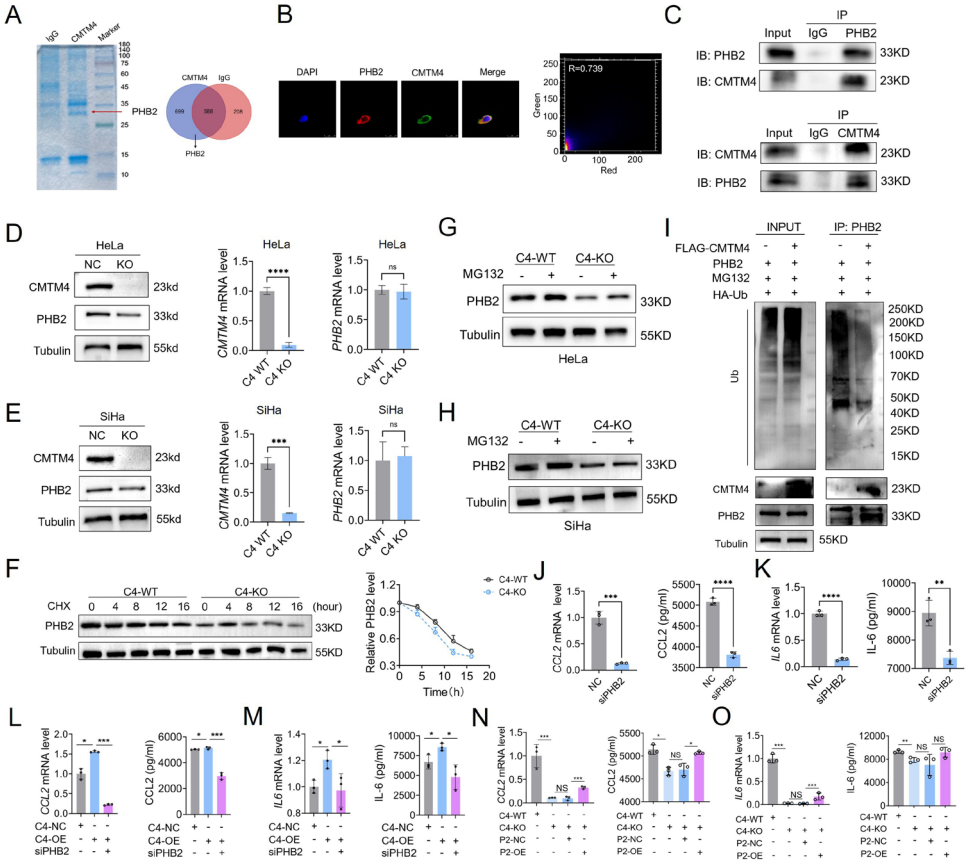

Figure 5 CMTM4 regulates the stability of PHB2. (A) Co-IP of HeLa protein lysates with anti-CMTM4 or anti-IgG, followed by Coomassie staining and LC-MS/MS identification of 699 potential interactors. (B) Immunofluorescence analysis of colocalization of CMTM4 and PHB2. HeLa is transfected with Flag-tagged CMTM4 (green) and HA-tagged PHB2 (red). ImageJ analysis of localization correlation between CMTM4 and PHB2. (C) Endogenous Co-IP showing CMTM4-PHB2 interaction. (D–E) PHB2 protein or mRNA levels in CMTM4-KO HeLa and SiHa. (F) CHX chase assay in HeLa-C4KO cells showing PHB2 half-life. (G–H) MG132 (10 µM, 6 hours) rescues PHB2 degradation in CMTM4-KO HeLa and SiHa. (I) Reduced PHB2 ubiquitination in 293T cells co-expressing CMTM4. (J–K) The expression of CCL2 or IL-6 in HeLa with or without PHB2 knockdown. (L–M) The expression of CCL2 or IL-6 in CMTM4-OE HeLa with or without PHB2 knockdown. (N–O) The expression of CCL2 or IL-6 in CMTM4-KO HeLa with or without PHB2 overexpression. *p<0.05, **p<0.01, ***p<0.001, ****p<0.0001, NS, not significant. CCL2, C-C motif chemokine ligand 2; CHX, cycloheximide; CKLF, chemokine-like factor; CMTM, CKLF-like MARVEL transmembrane domain-containing family; Co-IP, co-immunoprecipitation; DAPI, 4′,6-diamidino-2-phenylindole; FLAG, FLAG epitope tag; HA-Ub, hemagglutinin-tagged ubiquitin; IB, immunoblotting; IL-6, interleukin-6; IP, immunoprecipitation; KO, knockout; LC-MS/MS, liquid chromatography-tandem mass spectrometry; mRNA, messenger RNA; NC, negative control; OE, overexpression; PHB2, prohibitin 2; siPHB2, small interfering RNA targeting prohibitin 2; WT, wild type.

this phenomenon is not as pronounced as MDSCs recruitment through the CCL2/CCR2 axis, indicating that CMTM4 primarily facilitates the occurrence and development of CC by recruiting MDSCs through the CCL2-CCR2 axis.

CMTM4 regulates the stability of PHB2

To investigate the molecular basis of CMTM4 upregulation of CCL2/IL-6 expression in CC cells, we performed co-immunoprecipitation (Co-IP) in HeLa cells, followed by liquid chromatography-tandem mass spectrometry (LC-MS/MS) analysis, identifying that prohibitin 2 (PHB2) was co-purified with CMTM4 (figure 5A). Immunofluorescence confirmed their cytoplasmic co-localization (figure 5B), which was further validated by endogenous (figure 5C) and exogenous Co-IP methods (online supplemental figure 7A). To explore the possible regulatory effect of CMTM4 on PHB2, we evaluated the protein and transcriptional levels of PHB2 in C4WT or C4KO CC cells. WB analysis revealed reduced PHB2 protein levels in CMTM4-knockout HeLa and SiHa cells, whereas PHB2 mRNA remained unchanged (figure 5D,E), suggesting CMTM4 stabilizes PHB2 post-translationally.

Cycloheximide chase assays revealed that CMTM4 knockout significantly shortened the half-life of endogenous PHB2 in HeLa cells (figure 5F), indicating the protective effect of CMTM4 against PHB2 degradation. This stabilization was mediated through the ubiquitin-proteasome pathway, as evidenced by the ability of the proteasome inhibitor MG132 to rescue PHB2 protein levels in both HeLa and SiHa CMTM4-knockout cells (figure 5G,H). Further mechanistic studies showed that

CMTM4 overexpression reduced polyubiquitin chains on PHB2 in vitro (figure 5I).

We next proceeded to establish the biological relevance of the CMTM4-PHB2 interaction through the overexpression or knockdown of PHB2 in HeLa cells (online supplemental figure 7B–E). Knockdown of PHB2 resulted in the downregulation of CCL2 and IL-6 at both the transcriptional and protein levels (figure 5J,K). Functionally, PHB2 knockdown abrogated CMTM4-overexpression induced CCL2/IL-6 upregulation (figure 5L,M), while PHB2-overexpression rescued cytokine expression in CMTM4-knockout cells (figure 5N,O), establishing PHB2 as the key mediator of CMTM4's effects on CCL2/IL-6 production.

CMTM4 regulates the expression of CCL2/IL-6 by PHB2 and activating the STING/TBK1/STAT6 pathway

PHB2, a member of the PHB family, plays a role in various cellular processes, including cell proliferation, apoptosis, mitochondrial autophagy, and metastasis.[19] It has recently been identified as a novel target for regulating mitochondrial autophagy[20–22] and reported as an oncogene.[23–25] Studies have indicated that mitochondrial autophagy might facilitate the release of inflammatory factors through the STING/TBK1/STAT6 pathway.[26 27] Therefore, we hypothesize that CMTM4 can regulate the expression of CCL2/IL-6 through the PHB2-induced STING/TBK1/STAT6 axis. We found that CMTM4 knockout in HeLa cells reduced phosphorylation of STING (Ser365), TBK1 (Ser172), and STAT6 (Tyr641) without affecting their basal levels (figure 6A). This reduction was also observed in HeLa-PHB2-knockdown cells (figure 6B), while PHB2 overexpression in CMTM4-knockout cells restored pathway activation (figure 6C). Additionally, CMTM4 overexpression enhanced phosphorylation of these signaling molecules, an effect abolished by PHB2 knockdown (figure 6D). These results suggest that CMTM4 regulates the STING/TBK1/STAT6 pathway by targeting PHB2.

To assess the role of the STING/TBK1/STAT6 pathway in regulating CCL2/IL-6, we inhibited STING/TBK1/STAT6 signaling using H-151 and conducted rescue verification (figure 6E,F). Subsequent results indicated that blocking this pathway led to a downregulation of CCL2/IL-6 transcription and protein levels (online supplemental figure 8A–D), which reversed the upregulation of CCL2/IL-6 mediated by CMTM4 overexpression (figure 6G,H).

CMTM4 induces nuclear translocation of p-STAT6^{Tyr641} and binding of STAT6 to the CCL2/IL-6 promoter to increase transcription of CCL2/IL-6

As a transcription factor, STAT6 primarily functions by translocating to the nucleus. Thus, we examined the nuclear translocation of STAT6 in HeLa-C4WT and HeLa-C4KO. CMTM4 knockout reduced STAT6 nuclear localization in HeLa cells (figure 6I,K). Furthermore, we observed that in cervical cancer tissues, STAT6 was mainly distributed in the nucleus, whereas in chronic cervicitis tissues, STAT6 was predominantly distributed in the cytoplasm (figure 6J). Next, we used the hTFtarget website to predict the potential binding sites of STAT6 with the CCL2/IL-6 promoter (online supplemental figures 9 and 10). Chromatin immunoprecipitation (ChIP) assays demonstrated CMTM4 knockout decreased STAT6 binding to CCL2/IL-6 promoters, reversible by PHB2 overexpression (figure 6L,M). These results establish that CMTM4 activates the STING/TBK1/STAT6 pathway through PHB2, induces the nuclear translocation of STAT6, and thereby binds to the CCL2/IL-6 promoter to increase the transcription of CCL2/IL-6.

Target CMTM4 potentiates the effect of anti-PD-1 therapy in suppressing CC

Previous research has indicated that CMTM4 promotes CC progression via immune modulation. This leads us to hypothesize that targeting CMTM4 could potentially influence how CC responds to immunotherapy. Analysis of immunotherapy-treated cohorts (melanoma, glioblastoma multiforme, non-small cell lung cancer) revealed elevated CMTM4 expression in non-responders[28] (figure 7A). Besides, The Cancer Genome Atlas data further showed higher CMTM4 levels in partial responders compared with complete responders, implicating CMTM4 in treatment resistance (figure 7B). More importantly, CMTM4 knockdown reduced PD-L1 expression in HeLa cells (online supplemental figure 11), consistent with its reported role in PD-L1 stabilization.

To test combinatorial potential, we structured an in vivo small interfering RNA targeting CMTM4 (siCMTM4), and treated TC1 allograft-bearing mice with siCMTM4 and/or anti-PD-1 (figure 7C). While both monotherapies inhibited tumor growth, their combination showed superior efficacy (figure 7D–F). The combination therapy demonstrated superior immunomodulatory effects, significantly reducing G-MDSCs (figure 7G,H, online supplemental figure 12A,B) and Tregs (figure 7I, online supplemental figure 12C,D) while promoting activated T cell infiltration (figure 7J, online supplemental figure 12E,F) compared with monotherapies.

Collectively, these findings establish CMTM4 blockade as a promising strategy to restore antitumor immunity and potentiate ICB efficacy in CC, positioning CMTM4 as a viable therapeutic target.

DISCUSSION

In this investigation, we identified a significant upregulation of CMTM4 within the CMTM family in CC, correlating with unfavorable prognostic outcomes. Elevated CMTM4 expression emerged as a pivotal factor guiding MDSCs homing to CC, predominantly fostering CCL2/CCR2-mediated MDSCs chemotaxis and IL-6/GP130-induced MDSCs differentiation. This orchestrated interplay resulted in diminished infiltration of $CD8^{+}IFN\text{-}\gamma^{+}$ T cells, fostering immune evasion and advancing CC progression.

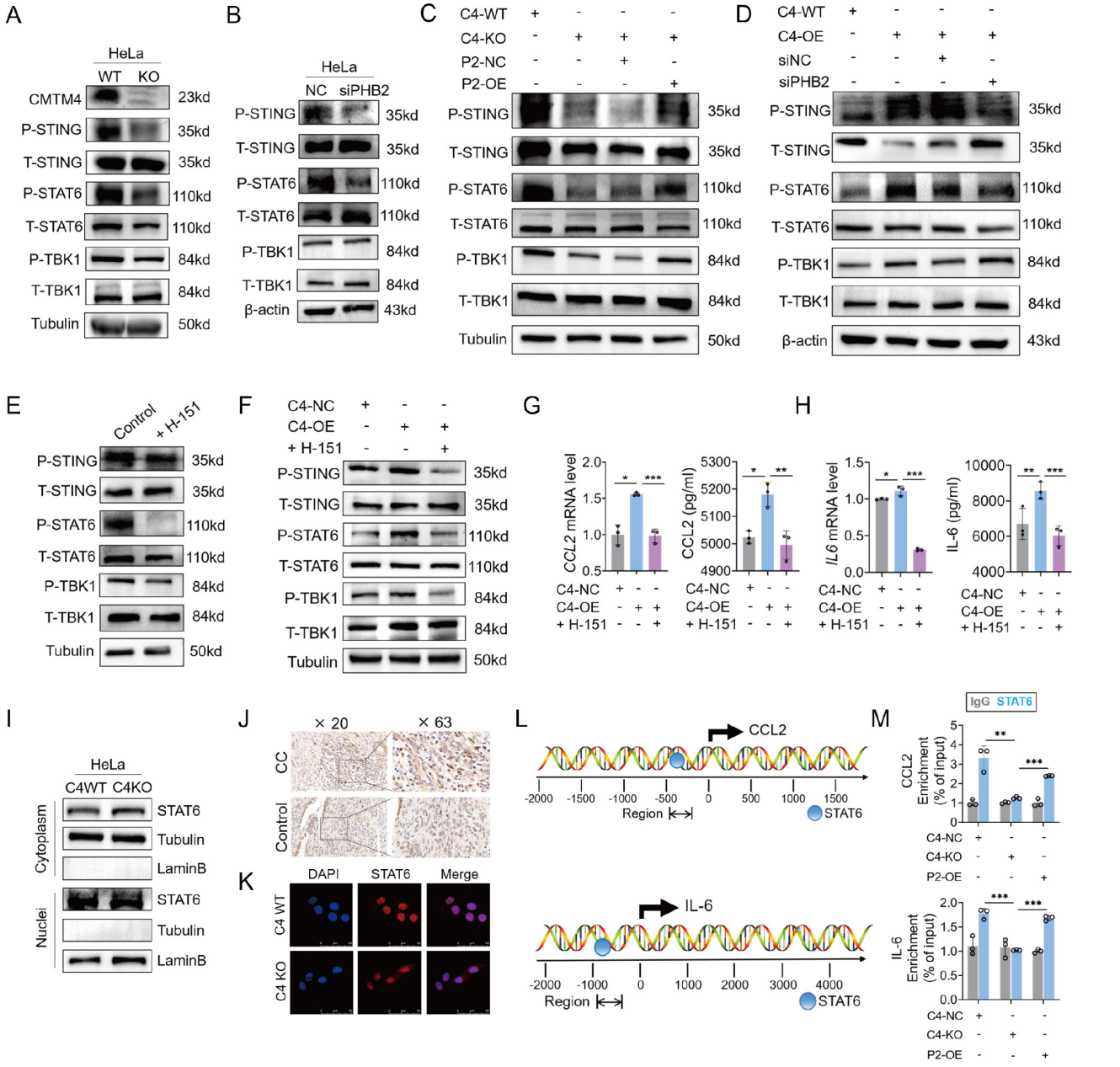

Figure 6 CMTM4 regulates CCL2/IL-6 expression through PHB2 and activation of the STING/TBK1/STAT6 pathway. (A) WB analysis of STING/TBK1/STAT6 pathway in HeLa cells with or without CMTM4 knockout. Tubulin was used as a control. (B) WB analysis of STING/TBK1/STAT6 pathway in HeLa cells with or without PHB2 knockdown. β-actin was used as a control. (C) WB analysis of STING/TBK1/STAT6 pathway in CMTM4-KO HeLa with or without PHB2 overexpression. β-actin was used as a control. (D) WB analysis of STING/TBK1/STAT6 pathway in CMTM4-OE HeLa with or without PHB2 knockdown. β-actin was used as a control. (E) WB analysis of STING/TBK1/STAT6 pathway in HeLa cells with or without treatment by H-151. β-actin was used as a control. (F) WB analysis of STING/TBK1/STAT6 pathway in CMTM4-OE HeLa with or without treatment by H-151. Tubulin was used as a control. (G–H) The expression of CCL2 or IL-6 in CMTM4-OE HeLa with or without PHB2 knockdown. (I) STAT6 level is tested in the nuclear and cytoplasmic fractions of CMTM4 NC-HeLa and CMTM4 KO-HeLa cells. Protein expression levels in the nuclear and cytosolic fractions were normalized to LaminB and Tubulin, respectively. (J) IHC analysis of benign controls and cervical cancer using specific antibodies for STAT6. Scale bar for×20 images: 50 µm; scale bar for×63 images: 20 µm. (K) IHC analysis of subcellular distribution of endogenous STAT6 in CMTM4 NC-HeLa and CMTM4 KO-HeLa cells. (L) The potential binding site of STAT6 to the CCL2 (up) or IL-6 (below) promoter is predicted by using the hTFtarget website. (M) ChIP assay analysis of STAT6 binding to the CCL2 (up) or IL-6 (below) promoter via the CMTM4/PHB2 pathway. *p<0.05, **p<0.01, ***p<0.001. CC, cervical cancer; CCL2, C-C motif chemokine ligand 2; ChIP, chromatin immunoprecipitation; CKLF, chemokine-like factor; CMTM, CKLF-like MARVEL transmembrane domain-containing family; DAPI, 4′,6-diamidino-2-phenylindole; IHC, immunohistochemical; IL-6, interleukin-6; KO, knockout; mRNA, messenger RNA; NC, negative control; OE, overexpression; PHB2, prohibitin 2; siNC, small interfering negative control; siPHB2, small interfering RNA targeting prohibitin 2; STAT6, signal transducer and activator of transcription 6; STING, stimulator of interferon genes; TBK1, TANK-binding kinase 1; WB, western blot; WT, wild type.

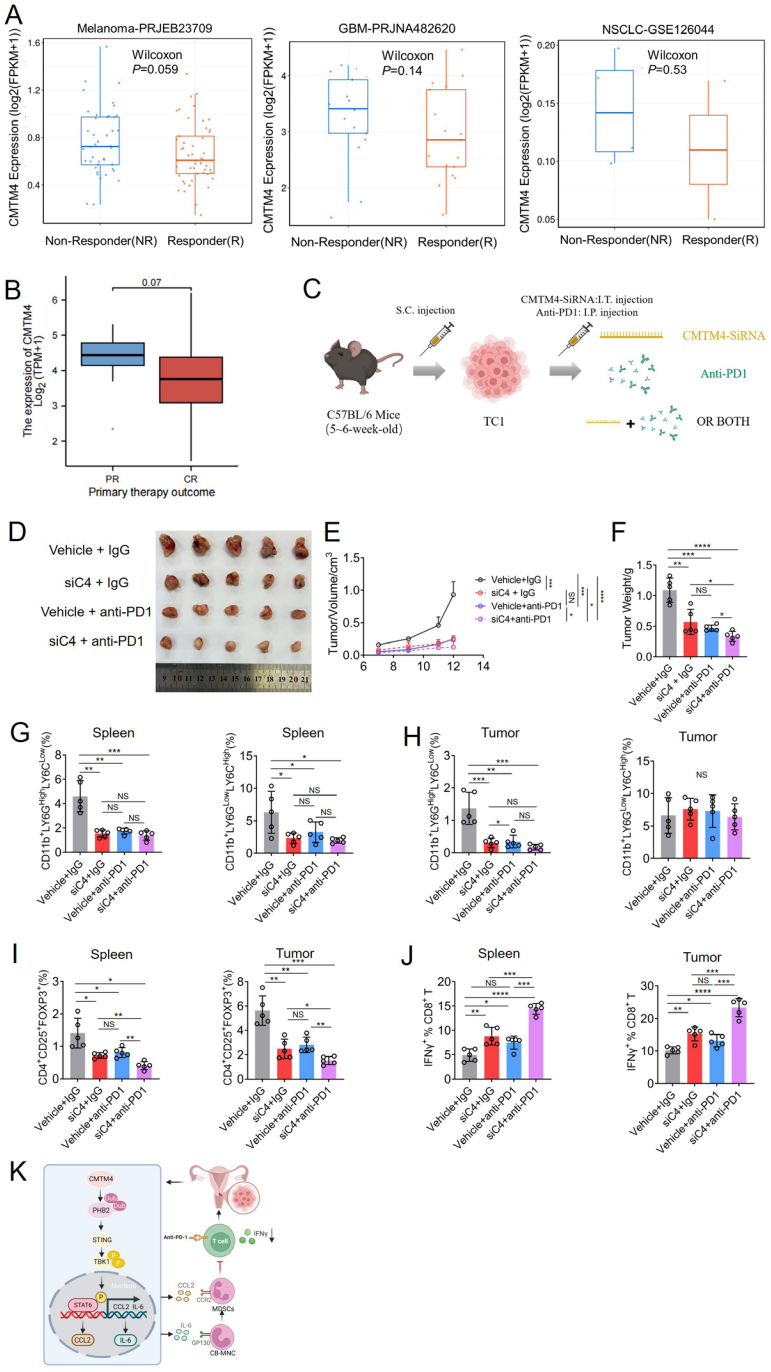

Figure 7 Targeted CMTM4 treatment enhances the efficacy of PD-1 blockade. (A) ICBatlas website analysis of expression level of CMTM4 in different subgroups (NR and R) of anti-PD-1 therapy-treated clinical cohort. (B) Expression level of CMTM4 in different subgroups (CR and PR) of prime therapy-treated TCGA clinical cohort. (C–D) Schematic showing the treatment plan: Tumor growth of TC1 tumor-bearing mice treated with CMTM4 siRNA, anti-PD-1 mAb alone or the anti-PD-1 mAb combined with the CMTM4 siRNA (Up, n=5/group). Images of TC1 allografts are shown (D). (E–F) Analysis of tumor growth and tumor weight is shown. (G–H) Flow cytometric analysis of $CD11b^{+}LY6G^{High}LY6C^{Low}$ G-MDSCs and $CD11b^{+}LY6G^{Low}LY6C^{High}$ M-MDSCs in spleens and tumors isolated from tumor-bearing mice. (I) Flow cytometric analysis of $CD4^{+}CD25^{+}FOXP3^{+}$ Tregs in spleens and tumors isolated from tumor-bearing mice. (J) Flow cytometric analysis of the infiltration of IFN-γ $CD8^{+}$ T cells in spleens and tumors. (K) Schematic representations of the role of CMTM4 in driving immune suppression in CC. *p<0.05, **p<0.01. ***p<0.001, ****p<0.0001. NS=No significance. CC, cervical cancer; CCL2, C-C motif chemokine ligand 2; CCR2, C-C motif chemokine receptor 2; CKLF, chemokine-like factor; CMTM, CKLF-like MARVEL transmembrane domain-containing family; CN-MNC, cord blood-derived mononuclear cell; CR, complete responders; GBM, glioblastoma multiforme; GP130, glycoprotein 130; IFN, interferon; IL-6, interleukin-6; I.P., intraperitoneal; I.T., intertumoral; mAb, monoclonal antibody; MDSC, myeloid-derived suppressor cell; NSCLC, non-small cell lung cancer; PD-1, programmed cell death protein 1; PHB2, prohibitin 2; PR, partial responder; S.C., subcutaneous; siRNA, small interfering RNA; STAT6, signal transducer and activator of transcription 6; STING, stimulator of interferon genes; TBK1, TANK-binding kinase 1; TCGA, The Cancer Genome Atlas.

CMTM4, belonging to the chemokine-like factor superfamily, has been implicated in the post-translational regulation of PD-L1, exerting inhibitory effects on effector T cells within TME and evading immune surveillance through the PD-1/PD-L1 signaling pathway.[5 10] Existing research has predominantly centered on CMTM4's regulation of PD-L1, impacting tumor initiation and progression. However, its influence on other facets of the immune milieu remains unclear, particularly in CC. Notably, in immunodeficient mice, the disparity in tumor growth between the C4 KO group and the control group is not as pronounced as observed in immunocompetent mice. This suggests that CMTM4's regulatory role in CC predominantly hinges on immune effects. Further exploration underscored CMTM4's principal impact on modulating MDSCs abundance and antitumor responses in vivo. To our knowledge, this study is the pioneering demonstration that the inhibition of CMTM4 in CC leads to a noteworthy reduction in CCL2 and IL-6, thereby mitigating MDSCs recruitment and enhancing the antitumor response in vivo. Furthermore, our analysis of clinical samples elucidated the relationship between CMTM4, CCL2, IL-6, and MDSCs.

Prior studies have highlighted the impact of CMTM4 on tumor proliferation and metastasis,[29] its role in maintaining the phenotype of tumor stem cells, and its promotion of epithelial-mesenchymal transition. Notably, CMTM4 has been implicated in enhancing the migration and invasion of head and neck squamous cell carcinoma.[30] However, contradictory reports also suggest tumor-suppressive effects of CMTM4 in certain cancers, such as its ability to inhibit cell proliferation in renal clear cell carcinoma.[31] In our in vitro functional experiments, we observed that CMTM4 promotes the proliferation and migration of CC. Intriguingly, findings from tumor-bearing mice with compromised immune function indicate that CMTM4 predominantly influences the onset and progression of cervical cancer through immune rather than non-immune mechanisms.

Despite reports highlighting CMTM4's negative regulation of cytotoxic T cells and its inhibition of T cell antitumor immunity by stabilizing PD-L1, its precise impact on other immune cells within the TME remains elusive. Our investigation involved the composition of immune cells within the TME in tumor-bearing mice, revealing that CMTM4 knockout significantly lowered the proportion of MDSCs and Treg cells, while concurrently elevating $CD8^{+}IFN\text{-}\gamma^{+}$ T cells. These results suggest that CMTM4 may predominantly exert its immunosuppressive effects by regulating MDSCs.

MDSCs are heterogeneous populations of myeloid progenitor cells derived from bone marrow to tumor sites, representing the main immunosuppressive population that only exists under pathological conditions such as chronic inflammation and cancer.[32] Within MDSCs, two distinct types, G-MDSCs, and M-MDSCs, exert immunosuppressive functions by impeding adaptive antitumor immunity, hindering T-cell proliferation and activation. Notably, G-MDSCs predominate in both human patients and animal models.[14] Our investigation revealed that CMTM4 deletion in CC compromises its capacity to facilitate the accumulation and suppressive functions of MDSCs, particularly G-MDSCs. Hence, the expansion of MDSCs emerges as a primary mechanism for CC to evade immune surveillance.

Chemokines and inflammatory factors play pivotal roles in MDSCs activation and recruitment to tumor sites through interactions with their corresponding receptors. Employing the KEGG (Kyoto Encyclopedia of Genes and Genomes) database for gene enrichment analysis of CMTM4-associated genes, our results suggest that CMTM4 may predominantly engage in the regulation of cytokine production. Combined with Luminex, Q-PCR, and ELISA assay, CCL2 and IL-6 were reduced after CMTM4 knockout in CC cells. CCL2, a major chemokine, orchestrates the recruitment of MDSCs to tumors through CCR2, while IL-6 induces MDSCs differentiation via GP130. Our assessment of CCR2 expression on MDSCs in tumor-bearing mice and clinical samples demonstrated significant upregulation in TC1-C4WT tumor-bearing mice compared with the TC1-KO group. Moreover, the expression of CCR2 on MDSCs in the peripheral blood of patients with CC significantly increased compared with the benign control group. Additionally, the expression level of GP130 in CB-MNC treated with IL-6 recombinant factor also significantly increased. Both in vitro and in vivo experiments further affirmed that CMTM4 recruits MDSCs through the CCL2/CCR2 axis, exerting a pivotal role in CC progression, and induces MDSC differentiation through the IL-6/GP130 axis.

Currently, the precise mechanism through which CMTM4 functions within tumor cells remains unclear. Our study employed LC-MS/MS analysis, revealing that CMTM4 interacts with PHB2, a finding subsequently validated through endogenous and exogenous Co-IP. Moreover, we observed that CMTM4 knockout led to a downregulation of PHB2 protein levels in CC cells, but no significant changes were detected in PHB2 mRNA levels. This indicates that CMTM4 regulates PHB2 expression through post-translational modifications. Consistently, we found that CMTM4 knockdown shortened the half-life of the CMTM4 protein. Furthermore, CMTM4 reduces the degradation of PHB2 in a proteasome-dependent manner. Additional experiments revealed that CMTM4 can regulate PHB2 expression by modulating its deubiquitination levels. All these findings suggest that CMTM4 may participate in the regulation of PHB2 stability and expression through post-translational modifications, although further investigation is needed to identify the specific deubiquitinating enzyme involved.

PHB2, one of the two proteins constituting prohibitins (PHBs), is a highly conserved protein with critical roles in transcription, epigenetic regulation, nuclear signaling, mitochondrial structural integrity, cell division, and membrane metabolism. Previous research has identified four primary functions of PHB2: (1) promoting

migration, (2) enhancing proliferation, (3) inducing anti-apoptosis and cell survival, and (4) initiating mitochondrial autophagy.[19] Notably, recent studies have underscored the pivotal role of PHB2 in mitochondrial autophagy.[20 22]

Studies have found that mitochondrial components and metabolites can function as damage-associated molecular patterns. They can induce inflammatory reactions through the STING pathway, and further promote the formation and progress of infectious diseases and tumors.[26] Although some studies have implicated the STING/TBK1/STAT6 pathway in the regulation of CCL2 expression,[27] and the STING pathway in the regulation of IL-6 expression,[33 34] there is currently a dearth of research exploring whether PHB2 is involved in the STING pathway and affects the expression of CCL2 and IL-6. Therefore, we investigated the potential for CMTM4 to regulate the STING pathway through PHB2. Our results demonstrated that CMTM4 can upregulate the expression of CCL2 and IL-6 by phosphorylating $STING^{S365}$/$TBK1^{Ser172}$/$STAT6^{Tyr641}$ through PHB2.

As a transcription factor, STAT6 has been reported to bind to the CCL2 promoter, thereby upregulating the transcription and expression of CCL2.[27] However, it remains unclear whether STAT6 regulates the activity of the IL-6 promoter. Our study demonstrates that CMTM4 knockout inhibits the nuclear translocation of STAT6 in HeLa cells. By predicting potential binding sites of STAT6 on the CCL2/IL-6 promoters using the hTFtarget website and validating them through ChIP assays, we provide evidence that CMTM4 targets PHB2 to phosphorylate STAT6, facilitating its nuclear translocation to bind to the promoters of CCL2 and IL-6, which leads to the upregulation of CCL2/IL-6 expression.

Currently, immunotherapy for CC is mostly single-agent treatment, and the efficacy is not satisfactory. Therefore, attempting to combine some molecular targeted drugs has become an emerging direction in the immunotherapy of CC. Advanced patients with CC exhibit an immune suppressive state, such as the accumulation of MDSCs, which significantly affects the efficacy of immunosuppressive therapies. In this context, we discovered that CMTM4 is highly expressed in CC and plays a crucial role in regulating the recruitment and differentiation of MDSCs. In in vivo treatment models, targeting CMTM4 resulted in significant inhibition of tumor growth. Moreover, the combination of siCMTM4 and anti-PD-1 therapy demonstrated a synergistic antitumor effect. Mechanistically, targeting CMTM4 led to a reduction in CCL2 and IL-6 expression, as well as decreased MDSC infiltration, which in turn enhanced the antitumor response mediated by $CD8^+$ T cells in conjunction with anti-PD-1 therapy. Our study suggests CMTM4 as a potential therapeutic target for combination therapy with ICI for CC treatment.

Nevertheless, we acknowledge several limitations in our study. We did not identify the upstream regulatory factors influencing CMTM4 expression, which hinders our understanding of the fundamental reasons for the differences in the formation of the TME. Addressing these issues will necessitate further research efforts.

In conclusion, our findings support the role of CMTM4 as a regulator of CC progression, at least in part through the PHB2/STING/TBK1/STAT6 pathway, which depends on the CCL2-CCR2 and IL-6-GP130 axes to recruit and differentiate MDSCs, thereby promoting immune escape in CC. Pharmacological blockade of the CCL2-CCR2 and IL-6-GP130 axes can inhibit tumorigenesis and progression, but not in CMTM4 knockout tumor models. The combination of CMTM4 inhibition and anti-PD-1 therapy demonstrates promising antitumor efficacy against CC, suggesting that CMTM4 could serve as a potential target for immunotherapy in the context of CC. Further research and development in this direction may open new avenues for therapeutic interventions in CC.

MATERIALS AND METHODS

Human samples

Clinical samples were collected and stored in Shanghai First Maternity and Infant Hospital from February 2020 to July 2023. All patients provided informed consent for providing the samples. Immunofluorescence staining of CMTM4 on CC tissue microarray was conducted by Xi'an Elena Biotechnology Company, and the staining percentages were calculated accordingly. CMTM4 positive area was determined by ImageJ. Peripheral blood was obtained from patients before surgery, and peripheral blood mononuclear cells (PBMCs) were separated by density gradient centrifugation (Ficoll Paque Plus; GE Healthcare, USA) and used directly for subsequent experiments.

Cell culture and transfection

A human cervical immortalized squamous cell line (Ect1/E6E7) and human cervical cancer cell lines (HeLa, SiHa, 293T, TC1) were provided by the American Type Culture Collection (USA). HeLa, SiHa, TC1, and 293T cells were cultured in Dulbecco's Modified Eagle Medium (Gibco, USA). Immune cells were cultured in RPMI-1640 medium (Gibco, USA). All cells were maintained at 37°C in a 5% CO_2 incubator. The medium was supplemented with 10% FBS (fetal bovine serum), 100 µg/mL penicillin, and 100 µg/mL streptomycin.

Single guide RNAs (sgRNAs) were designed by the Zhang Lab of Technology CRISPR Design tool (https://zlab.squarespace.com/) and cloned into lentiCRISPR V.2. SgRNA sequences used are shown in online supplemental table 2. For lentivirus production, 8 µg of plasmid DNA, 6 µg of psPAX2, 2 µg of pMD2.G, and 36 µL of PEI (Servicebio, China) were mixed and added to 293T cells in a 10 cm culture dish. Media was changed 6 hours after transfection, and the supernatant was collected at 48 and 72 hours post-transfection. Next, the targeted cells were infected with the viral solution using the co-transfection reagent Polybrene 8 ug/mL (Geneseed, China). Puromycin was added to kill the untransfected cells 48 hours later, and the remaining cells were the stably transfected

cell lines. Single cells were isolated by limiting dilution and cultured again on 96-well plates (catalog no. 655180, Greiner Bio-One) for 8 days under the same conditions described in the section above, followed by expansion. Finally, CMTM4 expression deficiency was confirmed using immunoblotting analysis.

CCL2–small interfering RNA (siRNA) (Hanbio, Shanghai, China), PHB2-siRNA (Hanbio, Shanghai, China), and a non-targeting RNA were used. Cells were transfected using Lipofectamine 2000 Reagent (Invitrogen, Carlsbad, California, USA). Overexpression of human CMTM4 GV657-oeCMTM4-FLAG-Puro and overexpression of human PHB2 GV741-oePHB2-HA-Puro was designed and synthesized by Genechem (Shanghai, China). Cells were transfected using Lipofectamine 3000 Reagent (Invitrogen, Carlsbad, California, USA).

Mice and tumor models

CMTM4 knockout or control TC1 cells were injected subcutaneously into the dorsal flank of each 6-week-old female C57BL/6 or NOD/ShiltJ-Prkdc em26Cd52-Il2rg-em26Cd22 (NCG) mice, respectively. Tumor sizes were measured every 3 days. 20 days after tumor engraftment, mice were sacrificed to assess tumor development. All animal studies were approved by the Animal Experimentation Ethics Committee of Tongji University.

INCB3344 (catalog no. HY-50674, MCE) (10 mg/kg body weight), LMT-28 (catalog no. HY-102084, MCE) (10 mg/kg body weight), or DMSO was given daily via intraperitoneal injection following tumor inoculation in C57BL/6 mice.

TC1 cells were injected subcutaneously into the dorsal flank of 6-week-old female C57BL/6 mice. Starting from day 7, anti-PD-1 monoclonal antibody (catalog no. SOB0594, STARTER) or IgG isotype control (catalog no. S0B0788, STARTER) was given via intraperitoneal injection (100 µg/injection every 3 days). Si-CMTM4 (GenePharma, Shanghai, China) or Negative control (GenePharma, Shanghai, China) was administered via intertumoral injection (50 µg/tumor every 3 days). Tumors were measured every other day and weighed on harvesting.

Real-time quantitative PCR

Total RNA was extracted from cells and tissues using RNAiso Plus (Takara, Japan). Complementary DNA was synthesized from total RNA using ABScript III RT Master Mix for PCR (ABclonal, Wuhan, China) reagent. RT-qPCR was performed using QuantStudioTM Design and Analysis Software V.1.3.1 PCR System with Genious 2X SYBR Green Fast qPCR Mix (Low Rox Premixed) (ABclonal, Wuhan, China) following the manufacturer's instructions. All gene expression values were normalized to β-actin or GAPDH (glyceraldehyde-3-phosphate dehydrogenase) and calculated using a $2^{-\Delta\Delta Ct}$ Method. Primers used are listed in online supplemental table 3.

Western blot

Proteins from lysed cells were fractionated by SDS-PAGE (sodium dodecyl sulfate–polyacrylamide gel electrophoresis) and transferred to PVDF (polyvinylidene difluoride) membrane (Millipore, USA). Non-specific binding sites were blocked with 5% BSA (bovine serum albumin) in TBST (Tris-buffered saline with Tween 20) (120 mM Tris–HCl (Tris(hydroxymethyl)aminomethane hydrochloride) ((pH 7.4), 150 mM NaCl (sodium chloride), and 0.05% Tween 20 (polyoxyethylene (20) sorbitan monolaurate)) for 1.5 hours at room temperature. Blots were incubated with a specific antibody overnight at 4°C. WB of β-actin or GAPDH on the same membrane was used as a loading control. The membranes were then washed with TBST three times and incubated with an HRP (horseradish peroxidase)-conjugated secondary antibody. Proteins were visualized using an Immobilon Western Chemiluminescent HRP substrate (Millipore, USA). The extraction of nuclear protein was carried out using the nuclear and cytoplasmic protein extraction kit (catalog no. PK10014, Proteintech), following the manufacturer's instructions. Antibodies used in this study are listed in online supplemental table 4.

Flow cytometry

Immune cell composition from the spleen, PBMCs, and tumors were analyzed by flow cytometry for MDSCs, G-MDSCs, M-MDSCs, T cells, Th1, Th2, Th17, NK cells, macrophages, and dendritic cells. Single cells were treated with Cell Activation Cocktail (catalog no. 423303, BioLegend) or Brefeldin A Solution (1000X) (catalog no. 420601, BioLegend) for 6 hours, before detecting the secretion of T cells or MDSCs related factors. Intracellular Staining Perm Wash Buffer (10X) Kit was used to detect cytokine secretion. True-Nuclear Transcription Factor Buffer Set Kit was used to detect FOXP3 expression. Data were analyzed by Flowjo V.10.8.1. The antibody panels for characterizing different immune cell types are provided in online supplemental table 5.

Luminex-MultiDTX-43-Human Assay

CM from CMTM4 KO-HeLa and CMTM4 NC-HeLa were collected for the analysis of 43 human cytokines using Luminex-MultiDTX-43-Cytokine-Human immunoassay (LabEx, Univ) following the manufacturer's protocol.

ELISA

Different groups of cells were seeded at a density of 1.5×10^5 with 500 µL of the corresponding medium in 24-well plates. Cell culture supernatants were collected after 48 hours with a 0.45 µm Millex filter (catalog no. SLHVR33RS, Merck Millipore) and used for ELISA. These supernatants were also used for transwell and monocyte differentiation assays (described in detail below) as the cell–conditioned medium (CM). Human CCL2 or IL-6 protein levels in culture supernatants, and serum samples were measured using the Human CCL2/MCP-1 ELISA Kit (catalog no. 510026, Absin) or Human

IL-6 ELISA Kit (catalog no. 510003, Absin). Human Arg-1 or INOS protein levels in culture supernatants, and serum samples were measured using the Human Arg-1 ELISA Kit (catalog no. RK07687, Abclonal) or Human INOS ELISA Kit (catalog no. RK01945, Abclonal). Mice CCL2 or IL-6 protein levels in serum samples were measured using the Mouse Monocyte Chemotactic Protein 1 ELISA Kit (catalog no. RK00381, Abclonal, Wuhan, China) or Mouse IL-6 Quantikine ELISA Kit (catalog no. RK00008, Abclonal, Wuhan, China). The absorbance readings at 570 nm were subtracted from the readings taken at 450 nm using an iMark microplate reader (Bio-Rad) to establish standard curves for the calculation of the concentration. Microsoft Excel was used for analysis.

MDSCs isolation by magnetic bead cell sorting

Isolation of $CD11b^{+}CD33^{+}HLADR^{-}$total human MDSCs was performed by using CD33 magnetic bead (130-045-501; Miltenyi Biotec) and isolation of $CD11b^{+}Gr\text{-}1^{+}$ total mouse MDSCs was performed by using mouse MDSCs isolation kit (130-094-538; Miltenyi Biotec) according to the manufacturer's instruction. Briefly, after Fc receptor blockade, cells were stained with biotin-conjugated Gr-1 antibody and further labeled with anti-biotin microbeads. Labeled cells were passed through the separation columns (Miltenyi Biotec) for magnetic cell separation. Retained cells were analyzed to assess MDSCs purity (>90%) by flow cytometry.

MDSCs transwell assay

In vitro migration of MDSCs was evaluated in 24-well plates with Transwell polycarbonate-permeable supports (8.0 µm, Corning). Freshly isolated splenic MDSCs or PBMC MDSCs (3×10^{5}, >90% purity) were seeded on the upper chambers of the inserts, after incubation with or without a CCR2 antagonist, RS504393 or a GP130 antagonist, LMT-28. The CM from CC cells was placed in the lower chamber with or without recombinant CCL1 protein (1 ng/mL) (catalog no. RP01411, Abclonal) or recombinant IL-6 protein (40 ng/mL) (catalog no. C610007, Sangon, Shanghai, China). After incubation for 24 hours, the MDSCs in the bottom compartment were counted.

Monocyte differentiation assays

Umbilical cord blood mononuclear cells were plated in 24-well plates at a density of 1.2×10^{5}, and 500 µL of CM of different groups (generated as described in the "ELISA" section) supplemented with 40 ng/mL GM-CSF (granulocyte-macrophage colony-stimulating factor) (catalog no. C610017, Sangon, Shanghai, China). Plates were incubated for 48 hours in an atmosphere of 5% CO_2 at 37°C, and MDSCs cells were then evaluated using flow cytometry, as described above.

Cell immunofluorescence staining

Cells were fixed by 4% formaldehyde solution for 15 min. Triton X-100 (0.2%) was used to permeabilize the cell membrane for 30 min. Next, the cells were blocked in blocking solution at room temperature for 1 hour, and the primary antibodies were added and incubated overnight at 4°C. Then, the fluorophore-tagged secondary antibodies were incubated for 1 hour at room temperature. After that, the nuclei were counterstained with DAPI for 15 min and photographed with a confocal microscope.

Immunoprecipitation and mass spectrometry

Protein lysate from HeLa cells was immunoprecipitated using anti-CMTM4–agarose, and anti-IgG–agarose by IP/CoIP Kit (catalog no. abs955, Absin). The immunoprecipitates were then eluted and immunoblotted. The immunoprecipitation of CMTM4 interacting protein was visualized by Coomassie blue staining (catalog no. G2059, Servicebio, Wuhan, China). Potential CMTM4 targets identified by LC-MS/MS (Oebiotech). Protein lysate from HeLa cells was immunoprecipitated using anti-CMTM4–agarose or anti-PHB2–agarose. The immunoprecipitate was then eluted, and immunoblotted using anti-CMTM4 and anti-PHB2 antibodies. 293T cells were transfected with Flag-tagged CMTM4 and HA-tagged PHB2 for 48 hours. Cell lysates were immunoprecipitated with either anti-Flag antibody or anti-HA antibody, and the immunocomplexes were probed with the indicated antibodies.

Ubiquitination assay

293T cells with or without Flag-tagged CMTM4 were transfected with HA-Ub and PHB2 overexpression by using Lipofectamine 2000 reagent (Invitrogen) and the cells were then treated with MG132 (10 µM) for 6 hours before collection. Whole-cell lysates were subjected to immunoprecipitation with PHB2 antibody and western blotting with ubiquitination antibody to detect ubiquitinated PHB2.

Chromatin immunoprecipitation assay

Cells were crosslinked using 1% formaldehyde for 10 min at 37°C. After cell lysis, the DNA was fragmented by sonication. ChIP grade STAT6 antibody (catalog no. 5397S, Cell Signaling Technology) or IgG (catalog no. AC042, ABclonal, Wuhan, China) was used to immunoprecipitate the fragment DNA. Then, RT-qPCR was used to amplify the corresponding binding site on the promoters. The ChIP primers used in this study are provided in online supplemental table 6.

Statistical analysis

All results were expressed as mean±SD, unless otherwise indicated. To compare the difference between the two groups, the Mann-Whitney U test or Student's t-test were performed. To compare the differences among multiple groups, a one-way ANOVA (analysis of variance) test was performed. All statistical tests were performed using GraphPad Prism V.9.0 (GraphPad Software, San Diego, California, USA)

and a two-tailed p value of 0.05 was considered statistically significant.

Author affiliations
[1]Department of Gynecology, Shanghai Key Laboratory of Maternal Fetal Medicine, Shanghai Institute of Maternal-Fetal Medicine and Gynecologic Oncology, Shanghai First Maternity and Infant Hospital, School of Life Science and Technology, Tongji University, Shanghai 200092, China
[2]Department of Gynecology, Shanghai Tenth People's Hospital, School of Medicine, Tongji University, Shanghai, China
[3]Department of Gynecology, The First Affiliated Hospital of Wenzhou Medical University, Wenzhou, Zhejiang, China
[4]School of Life Science and Technology, Tongji University, Shanghai, China

Acknowledgements We thank all of the authors who contributed to the knowledge reviewed in this article.

Contributors LH, WW, and AL conceived the project and designed the experiments. JD and HH wrote the manuscript. JD, HH, and YZ performed most of the experiments and analyzed the data. XX and BY assisted with the experiments and provided technical help. BH, HZ, MY, TH, ML, YK, and ZR provided comments and assisted with manuscript preparation. LH is the guarantor.

Funding This work was supported by grants from the National Natural Science Foundation of China (81972422; 82403164; 82073172; 81572546).

Competing interests None declared.

Patient consent for publication Not applicable.

Ethics approval The study was approved by the Ethics Committee of Shanghai First Maternity and Infant Hospital, with the ethics approval number: KS21299. Participants gave informed consent to participate in the study before taking part.

Provenance and peer review Not commissioned; externally peer reviewed.

Data availability statement All data relevant to the study are included in the article or uploaded as supplementary information. Not applicable.

ORCID iD
Lingfei Han http://orcid.org/0000-0003-1914-0436

REFERENCES

1 Bray F, Ferlay J, Soerjomataram I, *et al*. Global cancer statistics 2018: GLOBOCAN estimates of incidence and mortality worldwide for 36 cancers in 185 countries. *CA Cancer J Clin* 2018;68:394–424.
2 Chambers D, Simpson L, Hill-Briggs F, *et al*. Proceedings of the 8th Annual Conference on the Science of Dissemination and Implementation: Washington, DC, USA. 14-15 December 2015. *Implement Sci* 2016;11 Suppl 2:100.
3 Han W, Ding P, Xu M, *et al*. Identification of eight genes encoding chemokine-like factor superfamily members 1-8 (CKLFSF1-8) by in silico cloning and experimental validation. *Genomics* 2003;81:609–17.
4 Plate M, Li T, Wang Y, *et al*. Identification and characterization of CMTM4, a novel gene with inhibitory effects on HeLa cell growth through Inducing G2/M phase accumulation. *Mol Cells* 2010;29:355–61.
5 Mezzadra R, Sun C, Jae LT, *et al*. Identification of CMTM6 and CMTM4 as PD-L1 protein regulators. *Nature New Biol* 2017;549:106–10.
6 Burr ML, Sparbier CE, Chan Y-C, *et al*. CMTM6 maintains the expression of PD-L1 and regulates anti-tumour immunity. *Nature New Biol* 2017;549:101–5.
7 Chen L, Yang Q-C, Li Y-C, *et al*. Targeting CMTM6 Suppresses Stem Cell-Like Properties and Enhances Antitumor Immunity in Head and Neck Squamous Cell Carcinoma. *Cancer Immunol Res* 2020;8:179–91.
8 Guan X, Zhang C, Zhao J, *et al*. CMTM6 overexpression is associated with molecular and clinical characteristics of malignancy and predicts poor prognosis in gliomas. *EBioMedicine* 2018;35:233–43.
9 Miao B, Hu Z, Mezzadra R, *et al*. CMTM6 shapes antitumor T cell response through modulating protein expression of CD58 and PD-L1. *Cancer Cell* 2023;41:1817–28.
10 Chui NN-Q, Cheu JW-S, Yuen VW-H, *et al*. Inhibition of CMTM4 Sensitizes Cholangiocarcinoma and Hepatocellular Carcinoma to T Cell-Mediated Antitumor Immunity Through PD-L1. *Hepatol Commun* 2022;6:178–93.
11 Peng Q-H, Wang C-H, Chen H-M, *et al*. CMTM6 and PD-L1 coexpression is associated with an active immune microenvironment and a favorable prognosis in colorectal cancer. *J Immunother Cancer* 2021;9:e001638.
12 Long Y, Chen R, Yu X, *et al*. Suppression of Tumor or Host Intrinsic CMTM6 Drives Antitumor Cytotoxicity in a PD-L1-Independent Manner. *Cancer Immunol Res* 2023;11:241–60.
13 Veglia F, Sanseviero E, Gabrilovich DI. Myeloid-derived suppressor cells in the era of increasing myeloid cell diversity. *Nat Rev Immunol* 2021;21:485–98.
14 Wu Y, Yi M, Niu M, *et al*. Myeloid-derived suppressor cells: an emerging target for anticancer immunotherapy. *Mol Cancer* 2022;21:184.
15 Flores-Toro JA, Luo D, Gopinath A, *et al*. CCR2 inhibition reduces tumor myeloid cells and unmasks a checkpoint inhibitor effect to slow progression of resistant murine gliomas. *Proc Natl Acad Sci U S A* 2020;117:1129–38.
16 Loyher P-L, Rochefort J, Baudesson de Chanville C, *et al*. CCR2 Influences T Regulatory Cell Migration to Tumors and Serves as a Biomarker of Cyclophosphamide Sensitivity. *Cancer Res* 2016;76:6483–94.
17 Li Z-W, Sun B, Gong T, *et al*. GNAI1 and GNAI3 Reduce Colitis-Associated Tumorigenesis in Mice by Blocking IL6 Signaling and Down-regulating Expression of GNAI2. *Gastroenterology* 2019;156:2297–312.
18 Sander LE, Sackett SD, Dierssen U, *et al*. Hepatic acute-phase proteins control innate immune responses during infection by promoting myeloid-derived suppressor cell function. *J Exp Med* 2010;207:1453–64.
19 Qi A, Lamont L, Liu E, *et al*. Essential Protein PHB2 and Its Regulatory Mechanisms in Cancer. *Cells* 2023;12:1211.
20 Yan C, Gong L, Chen L, *et al*. PHB2 (prohibitin 2) promotes PINK1-PRKN/Parkin-dependent mitophagy by the PARL-PGAM5-PINK1 axis. *Autophagy* 2020;16:419–34.
21 Liu L, Bai F, Song H, *et al*. Upregulation of TIPE1 in tubular epithelial cell aggravates diabetic nephropathy by disrupting PHB2 mediated mitophagy. *Redox Biol* 2022;50:102260.
22 Wei Y, Chiang WC, Sumpter R, *et al*. Prohibitin 2 Is an Inner Mitochondrial Membrane Mitophagy Receptor. *Cell* 2017;168:224–38.
23 Wu B, Chang N, Xi H, *et al*. PHB2 promotes tumorigenesis *via* RACK1 in non-small cell lung cancer. *Theranostics* 2021;11:3150–66.
24 Ren L, Meng L, Gao J, *et al*. PHB2 promotes colorectal cancer cell proliferation and tumorigenesis through NDUFS1-mediated oxidative phosphorylation. *Cell Death Dis* 2023;14:44.
25 Chu YD, Fan TC, Lai MW, *et al*. GALNT14-mediated O-glycosylation on PHB2 serine-161 enhances cell growth, migration and drug resistance by activating IGF1R cascade in hepatoma cells. *Cell Death Dis* 2022;13:956.
26 Marchi S, Guilbaud E, Tait SWG, *et al*. Mitochondrial control of inflammation. *Nat Rev Immunol* 2023;23:159–73.
27 Chen H, Sun H, You F, *et al*. Activation of STAT6 by STING is critical for antiviral innate immunity. *Cell* 2011;147:436–46.
28 Yang M, Miao Y-R, Xie G-Y, *et al*. ICBatlas: A Comprehensive Resource for Depicting Immune Checkpoint Blockade Therapy Characteristics from Transcriptome Profiles. *Cancer Immunol Res* 2022;10:1398–406.
29 Li M, Guo H, Wang Q, *et al*. Pancreatic stellate cells derived exosomal miR-5703 promotes pancreatic cancer by downregulating

CMTM4 and activating PI3K/Akt pathway. *Cancer Lett* 2020;490:20–30.
30 Li H, Liu Y-T, Chen L, *et al*. CMTM4 regulates epithelial-mesenchymal transition and PD-L1 expression in head and neck squamous cell carcinoma. *Mol Carcinog* 2021;60:556–66.
31 Li T, Cheng Y, Wang P, *et al*. CMTM4 is frequently downregulated and functions as a tumour suppressor in clear cell renal cell carcinoma. *J Exp Clin Cancer Res* 2015;34:122.
32 Gabrilovich DI, Ostrand-Rosenberg S, Bronte V. Coordinated regulation of myeloid cells by tumours. *Nat Rev Immunol* 2012;12:253–68.
33 Hong C, Schubert M, Tijhuis AE, *et al*. cGAS-STING drives the IL-6-dependent survival of chromosomally instable cancers. *Nature New Biol* 2022;607:366–73.
34 Sliter DA, Martinez J, Hao L, *et al*. Parkin and PINK1 mitigate STING-induced inflammation. *Nature New Biol* 2018;561:258–62.